PERGAMON

Journal of Structural Geology 21 (1999) 1071–1088

JOURNAL OF STRUCTURAL GEOLOGY

www.elsevier.nl/locate/jstrugeo

Can we understand structural and tectonic processes and their products without appeal to a complete mechanics?

Raymond C. Fletcher[a,*], David D. Pollard[b]

[a]*Department of Geological Sciences, University of Colorado, Boulder, CO 80309-0399, USA*
[b]*Department of Geological and Environmental Sciences, Stanford University, Stanford, CA 94305-2115, USA*

Received 15 April 1998; accepted 10 January 1999

Abstract

Our answer is 'no'. Throughout the 20th century, the majority of structural geologists have worked with a conceptual basis that includes only isolated fragments of continuum mechanics (e.g. strain analysis, constitutive laws, force balance, Mohr's circles, or conservation of volume), and this has resulted in the proliferation of ad hoc models of structural and tectonic processes and their products. Furthermore, at a more abstract level, the possibility that mechanical quantities of interest (e.g. displacement, velocity, stress, or temperature) vary continuously in the spatial coordinates and time is largely ignored. These two conceptual oversights are related: without the mathematical concept of partial differentiation (as in the biharmonic equation of elasticity theory that brings strain compatability, Hooke's law, and stress equilibrium together) these spatial and temporal variations cannot be accounted for explicitly. Thus, the mechanical concept of boundary- and initial-value problems, formulated in terms of partial differential equations, has not been adopted as a necessary tool by most practitioners of structural geology and tectonics. We illustrate our case with two examples: the development of chevron folds and of échelon veins. We show how the ad hoc approach, while successful at one level, lacks predictive capability and possesses a low degree of refutability. Further progress in understanding these (and other) products of structural and tectonic processes can be made through an integrative approach using a complete and self-consistent mechanics.

1. Introduction

> "...by the turn of the century it was fully realized that for an isotropic material the strain energy must involve the strain through the three strain invariants. It was also realized that if the form of this relationship were known for a particular material, stress–strain relations (or as we should now say, constitutive relations), equations of equilibrium, etc., and indeed the whole formalism for a *complete mechanics* of the material can be derived." Ronald S. Rivlin, in Barenblatt and Joseph (1996).

Structural geologists are concerned with the question (Dahlstrom, 1969): "What is the structure?" Geometric idealization of structure is made to facilitate interpolation and extrapolation from incomplete data throughout a volume. With the idea that restoration of a candidate structure to initial or earlier states provides a check on interpretation (Dahlstrom, 1969), methods of carrying this out were devised. The simplest such method may amount to tabulating bed lengths to determine whether, when carried back to a pin line, they all have the same value. A set of intermediate restored configurations may be produced, based upon constraints imposed by the available structural and geochronological data.

A second question is: What process produced the structure of interest? Even though a picture of the motions involved in going from a prior state to the final structure may be obtained from a postulated kinematic scheme, this does not provide a complete description of the process, since no causative physical principles are involved. A mechanist would be skeptical of the motions proposed, both in terms of their

* Corresponding author.
E-mail address: raymond.fletcher@colorado.edu (R.C. Fletcher)

0191-8141/99/$ - see front matter
PII: S0191-8141(99)00056-5

broader aspects and as to their capturing essential, but subtler, elements. In such kinematic modeling, the exclusive requirement is that the model fits observations of structural geometry, and any conflict with physical principles is ignored.

An unavoidable feature of such models is the adoption of a 'kinematic mechanism' capable of being written down in a simple algebraic form which relates the motion everywhere in the deforming medium to information at special positions within the structure. Put another way, the motion within the medium is obtained by applying a rule for transmitting information from a 'template' to any other point in the medium without degradation. For example, given the geometry of one layer surface in a folded sequence to be approximated using the *similar* template, all other surfaces are determined by a suitable translation of this surface along a line in the profile plane and parallel to the axial plane. As in this example, information is usually transmitted unidirectionally. Such schemes are fundamentally at odds with what happens in the physical world, in which causality dictates that local behavior be directly coupled to neighboring regions only by the pertinent *field equations*. Information on traction, velocity, or displacement, in a mechanical problem, on all bounding surfaces is transmitted throughout the interior by the application of the field equations.

Prompted by the comments of reviewers, two points require careful attention in advance. The first point concerns the role of fieldwork in providing a basis for mechanical modeling. A reviewer suggested that mechanical modeling applied to a particular structure or region builds on the extensive fieldwork carried out previously. Certainly, such work provides a basis for a particular line of investigation and may convey, explicitly, the problems outstanding. If, however, the fieldwork and interpretation are carried out with detailed kinematic interpretation, but no appeal to a complete mechanics, we commonly find that certain types of observations and sets of quantitative data are overlooked. An example might be the geometric details and extent and degree of fracturing and other damage in the region of interaction between two fault segments. Another example is the pattern of folding over a large cross-sectional area and the sequence of layer thicknesses and types in a folded multilayer. Such qualitative details and quantitative datasets will often firmly establish—or refute—postulates of a process model that will apply to a broad range of additional field examples.

The second point concerns the doubt, expressed by one reviewer, that a complete mechanical model has been developed if, in it, major simplifications or approximations are made—for example the use of 'frictionless faults' (Chester and Fletcher, 1997; Crider and Pollard, 1998). *Complete* does not imply the immediate simulation of all detail and complexity in the process leading to a particular structure or structural type. Instead, it requires that an explicit choice has been made of constitutive relations, boundary conditions, and initial conditions, which, together with the fundamental laws of physics, produces a closed set of relations from which all results follow. If the model results do not conform in all aspects with the current database, a more refined model may be formulated by a different choice of these mutable elements. The explanatory power of simpler models is first examined, often providing significant physical insight, then robustness as well as detailed simulation are pursued.

Studies of chevron folds and échelon veins illustrate the contrast between kinematic modeling, augmented by an incomplete mechanics, and a complete mechanical analysis employing the field equations. We begin by discussing the formulation and results of Ramsay's (1967, 1974; also Ramsay and Huber 1987), geometric, evolutionary, and kinematic model for chevron folds. Ramsay modified the model of de Sitter (1956) to better fit the geometrical attributes of the folds he observed. Others have given an analysis of chevron folding using a complete mechanics. For example, Bayly (1964), Cobbold (1976), and Casey and Huggenberger (1985) treat the layer sequence as a homogeneous anisotropic viscous medium. Williams (1980) presents finite-element and geometric models that take into account the discrete layers. We augment these studies with results from an analysis of a multilayer that describes buckling, kinematics, and aspects of the transition between sinusoidal and chevron form (see also Johnson and Pfaff, 1989; Pfaff and Johnson, 1989).

As a second example of the use of a complete mechanics to analyze a problem in structural geology, we turn to the subject of échelon veins. Early investigations of échelon fractures involved laboratory analogue experiments using clay cakes (Riedel, 1929; Cloos, 1955) and glass rods (Sommer, 1969). These experiments provided the motivation for the study of two different mechanisms for the formation of échelon vein segments: initiation within a shear zone (Ramsay, 1967) and propagation from the tip of a parent fracture (Pollard et al., 1982). We review this history, point out how much of the subsequent research involved incomplete mechanical analyses, and provide a specific example of a complete analysis by Olson and Pollard (1991). Finally, we review how a third mechanism, self-organization driven by mechanical interaction, was discovered during numerical experiments which provided visualization of the heterogeneous stress and strain fields near fractures.

2. The de Sitter–Ramsay model for chevron folds

Ramsay (1974) noted that mechanical modeling of folding up to that time had chiefly analyzed fold initiation, but that "structural geologists are also interested in the later stages of fold development and in how the geometric forms of the initial folds become modified as deformation proceeds…." Commenting upon laboratory and finite-amplitude numerical models, he noted:

> "The geometric results of these model experiments can be compared with those of naturally deformed rock layers. If the cross-section layer geometry and finite strain states are closely similar, then we might deduce that the rock behaved like the materials of the model, but it is possible to get the same approximate geometry from different materials undergoing different deformation histories. However, to many who have made detailed studies of naturally deformed rock layers, the correspondences between the model work and natural process are extremely close. I, for one, am convinced that this geometric correspondence is not just by chance."

Ramsay then clearly states the premise behind the altogether different approach from the complete mechanics of these fold modelers, that upon which all kinematic modeling is based. He states:

> "Although in general it is not possible to find the exact equations that account for progressive fold growth, field geologists know that certain styles of fold structure keep recurring, and some of them are geometrically fairly simple. Because of their simplicity, one is tempted to try to discover the functions that might express their evolutionary development. The chevron fold style is such an example, and in this paper, I attempt to make a geometric analysis of the progressive development of such folds. The concept behind this study is to set up a geometric model based on controls imposed by observations on naturally deformed, layered rocks, and then to investigate the properties of this model to see if any of its special geometric features help to aid an understanding of the geometric characteristics of naturally deformed rocks."

We make four points here. First, we assert that "the exact equations that account for progressive fold growth" are the field equations, including the constitutive postulates, and boundary and initial conditions used in a complete mechanical analysis. Second, it seems implausible that one may discover, by consideration of the geometric features of a structure alone, a functional form that fully describes its kinematic evolution. Third, how the 'simple' straight-limbed, narrow-hinged, chevron fold style originates itself constitutes a first-order problem. Fourth, the behavior of anomalously thick and thin layers in a folded sequence, a key 'prediction' of Ramsay's model, cannot be understood on the basis of purely geometric reasoning.

A more general point builds upon these. Many structural geologists would assert that mechanical analysis of structures is useful as an *additional* study, following one in which geometric and kinematic reasoning alone are brought to bear in the course of detailed study of deformed rocks. The latter methodology is that which is strongly advanced and lucidly illustrated in Ramsay's paper on chevron folds; none of his basic results are based upon mechanical reasoning. Later, as an after-thought, he derives additional results based on the postulate that the layers behave as linear viscous fluids. We assert that such a methodology is flawed for the reason that it leaves out essential concepts. These concepts are required not only to provide valid explanations for observed features, but also to motivate the detailed examination of the rocks and the collection of field data necessary to support, modify, or refute them.

2.1. Three levels in Ramsay's model

In Ramsay (1974), the de Sitter (1956) model and his earlier model (Ramsay, 1967) are extended to include the presence of weak interbeds. We discuss only the limiting case in which shearing in weak beds of finite thickness is replaced by interfacial slip.

De Sitter's and Ramsay's models have three hierarchical levels. The first level is that of geometric idealization. At the second level, an additional assumption is introduced that provides an evolutionary model describing the temporal sequence of fold form: constant limb length is assumed. At the third level, a detailed kinematics is proposed. We denote this the 'kinematic model.' Only at this level is the motion fully described, although the evolutionary model describes elements of it. All kinematic models may have this hierarchical structure.

The geometric model of de Sitter (1956) treats an infinite stack of layers of equal thickness. Two axial planes remain perpendicular to the initial limb segments at zero dip, isolating a single fold limb. Adjacent fold limbs must have mirror symmetry about the axial planes. Layer segments in de Sitter's model have length L and thickness H, with lateral faces normal to the layer surfaces. The geometric model has segments stacked with their extreme points just touching the axial planes.

In the evolutionary model, the layer segments are rigid, but slide relative to each other. The model is thus of the 'bookshelf' variety. At zero dip, the span

of the limb is L. At a dip θ, the distance between the axial planes is equal to the distance between the extreme points on the segments, and is given by

$$L(1+\varepsilon) = L\cos\theta + H\sin\theta \quad (1)$$

where ε is a measure of the bulk shortening strain (Ramsay, 1967), with $-1 < \varepsilon < 0$. The dilation in cross-sectional area per limb segment is given by

$$\Delta A/(LH) = v\tan\theta \cong v\theta \quad (2)$$

where $v = H/L$. Since the kinematics of folding is of the bookshelf type, the evolutionary and kinematic models coincide.

De Sitter's model does not explicitly address layer deformation in the hinge regions except, quoting Ramsay (1974), that he supposes that the layers "lose cohesion along the fold axial surface, thereby producing a series of dilational openings along the hinge zone." The layers of the natural chevron folds examined by Ramsay (1974) are continuous, have sharp inner hinge profiles, rounded outer hinge profiles, and uniform thickness around the hinges. Ramsay's model refines de Sitter's by eliminating its deficiency in approximating the fold form in the hinges.

Ramsay's model possesses the same hierarchical order of geometric, evolutionary, and kinematic models. This is not the manner in which he presents it. The significance of this order of presentation is twofold. First, we believe it is the way in which such models are usually conceived. They start with an idealization of the final geometry and move, via the evolutionary and kinematic models, back to some approximation of an initial, layered, but otherwise featureless, initial configuration. To reach the final structure, certain essential features must be introduced into the initial configuration, such as a system of bed-parallel faults and ramps. In the case of chevron folds, a pattern of incipient folds with straight limbs but very small dip must be posited. How this embryonic but controlling structure comes about is not addressed. Second, to the extent that a comparison can be made, this order is precisely the opposite of that in a complete mechanical model. Such a model goes forward from specified initial configuration and properties to generate the final structure, whose form is initially not even known. The stage of structure initiation is dealt with.

Ramsay's order of presentation is similar to that for a mechanical model. While the restrictions placed by field observations are first listed, the formal presentation begins with a statement of the mathematical relations defining the internal deformation of a single layer. Such kinematic rules are commonly associated with a mechanism of deformation, here, the shearing of inextensible but flexible sheets of infinitesimal thickness. Such a mechanism substitutes, approximately, for the constitutive relations in a complete mechanical model. The evolutionary model for folding is 'derived' by application of the kinematic model.

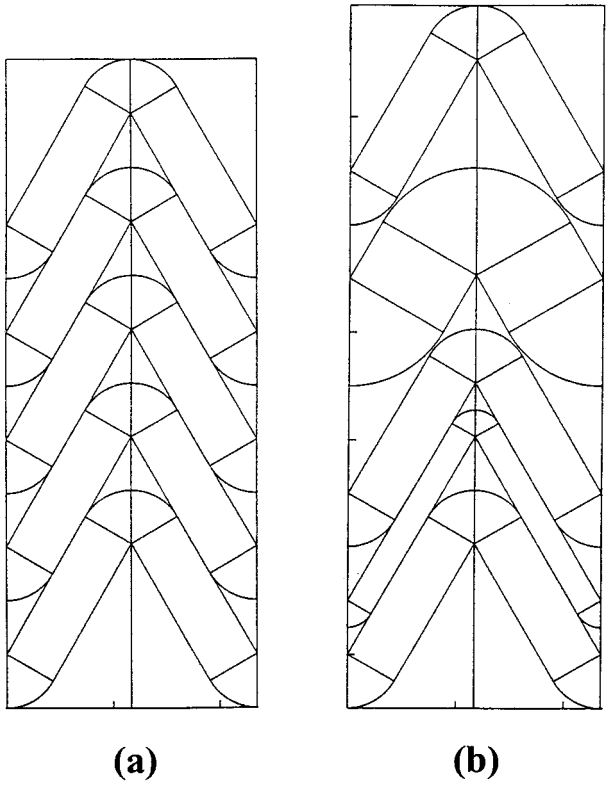

Fig. 1. Two examples of the geometric model for chevron folds. (a) Layers have equal thickness. (b) Layers have unequal thickness; while this geometric model might be used to idealize the form of a set of folded layers, it cannot be treated by Ramsay's evolutionary model.

In Ramsay's geometric model (Fig. 1a), each limb segment is idealized as a straight-sided layer segment, as in de Sitter's model. But, to bring the layer continuously through the hinges, circular sectors with radius equal to the layer thickness and with angle equal to the dip are added to the ends of each segment. Sector apices point in opposite directions, so that the outer hinge surfaces are smooth circular arcs and the inner hinge surfaces have a sharp angular discontinuity. Layer thickness through the hinges is uniform. The length of the limb, L, is the sum of the straight segment plus the circular arc. Note that we could readily describe the geometry of an idealized set of chevron folds with layers of different thickness by means of this model (Fig. 1b).

In the evolutionary model, the limb segments are assumed to maintain constant length. From a trigonometric analysis for a single layer in the folded sequence, we may derive the relation (Ramsay, 1974).

$$1+\varepsilon = (1-v\theta)\cos\theta + v\sin\theta. \quad (3)$$

Note the similarity to Eq. (1). This relation states that the bulk shortening at any dip is a function of $\nu = H/L$. Thus, folding of a sequence in which the layers are not of uniform thickness cannot be accommodated by this evolutionary model without mismatch along the limbs. Ramsay (1974, p. 1742) remarks:

> "Straight-limbed chevron folds are not geometrically stable where pronounced thickness variations occur in folds having constant limb length. This explains why chevron folds are generally localized in regularly bedded multilayer sequences such as are found, for example, in typical turbidite flysch deposits, and it also leads to an explanation of why the ratio of limb length to thickness of the competent layers generally exceeds 10/1."

Even equally thick layers do not fit together without dilation at the hinges. While this violates the constraint of conservation of cross-sectional area often applied in kinematic models, the dilation simulates the saddle reefs commonly seen in chevron folds, and is thus a point in favor of the model. The dilation

$$\Delta A/(LH) = \nu(\tan\theta - \theta) \cong \nu\theta^3/3 \tag{4}$$

is much smaller than that in the de Sitter (1956) model, Eq. (2).

Notice that the evolutionary model, the fundamental result of which is Eq. (3), neither depends upon how the layers initially achieve the idealized chevron form nor how they maintain it at constant limb length as the folds tighten. That is, the evolutionary model constrains the internal kinematics of the layer but does not determine it. Ramsay's kinematic model will be presented in a later section.

Up to this point, the model may have been worked out as we have presented it here. A geometric idealization was posed without restriction on layer thickness. The evolutionary behavior for a single layer of arbitrary initial thickness in the fold limb, expressed by Eq. (3), was obtained. It could then be seen that only layers of the same thickness would fit together. The inability of the model to accommodate layers of different thickness led Ramsay (1974) to the notion of 'geometrical stability'. This term merely expresses the inability of his evolutionary model to accommodate layers of unequal thickness. It has no apparent general significance, as for example, the principle of 'thermodynamic stability'.

2.2. 'Geometric stability' and the behavior of thicker and thinner layers

A striking feature in chevron folds (Ramsay, 1974) is the bulbous hinge structure produced in a much thicker layer within a stack of more-or-less uniformly thick layers. Anomalously thin layers show stretching, as indicated by bed-normal veins.

Consider the discrepancy when a sequence contains a layer with different thickness, $H^* \neq H$. Since the bulk shortening must be invariant through the stack, from Eq. (3)

$$(L - H^*\theta^*)\cos\theta^* + H\sin\theta^* = (L - H\theta)\cos\theta + H\sin\theta. \tag{5a}$$

Note that the limb length of the thicker layer is the same as that of the others. Since the discrepancy is small for moderate dips, we expand Eq. (5a) to lowest order in the dip angles, and write $\theta^* = \theta + \theta'$; we find

$$\theta' \cong (H^* - H)\theta^2/(3L). \tag{5b}$$

The limb dip is larger for a thicker layer; if $H^* = 4H$ and $L/H = 10$, the discrepancy is 1.6° at a dip of 30°. If the thick layer has the same dip, it will 'stick out' beyond the axial planes, since it achieved that dip at a lower bulk shortening. A bulbous hinge structure is formed by 'squeezing' the ends back in, with all adjustment in the hinge regions where room is provided by the space arising from dilation. A thinner layer, with $H^* < H$, has a lower dip at the same bulk shortening, and at the same dip will not reach the axial planes. More extension in a thinner layer is thus expected, possibly accommodated by layer-normal veins, as observed (Ramsay, 1974).

From Eq. (5b), the discrepancy in limb dip for unequal layer thickness in the stack is reduced for larger L/H values. Ramsay's observation that "chevron folds are generally localized in regularly bedded multilayer sequences" is rationalized by the consequence that, for such sequences, such discrepancies are minor.

Does the fact that this consequence of Ramsay's evolutionary model correlates with several observations from natural chevron folds imply that it explains them? It is important to critically examine this point, since such a result may equally well be carried over to other evolutionary models. A variant of Ramsay's model can accommodate layers of unequal thickness. The simplest version involves the uniform layer-parallel strain of the anomalous layer, resulting in a change in length from L to L^*. Conservation of area requires

$$L^*H^* = LH^*(0) \tag{6a}$$

where $H^*(0) = fH$ is the initial thickness of the anomalous layer and $L^*(0) = L$. The layer strain required to maintain the fit of the layer within the stack is

$$L^*/L - 1 = (1 - f)\nu(\tan\theta - \theta) \cong (1 - f)\nu\theta^3/3. \quad (6b)$$

Since, by Eq. (6b), any adjustment in length will only become quantitatively significant at a substantial limb dip, the fold pattern will have already been established by buckling.

Accordingly, two variants of the evolutionary model are consistent with the same geometric idealization. One does not accommodate layers of different thickness, but the other does. The latter model excludes the formation of bulbous hinge structures, but does describe the deformation of a thin layer. A model lying between these extremes might also admit the bulbous hinge structure. None describe the process that formed the folds.

In a geometric or mechanical model, no account is given of how the limb lengths of chevron folds are established. Ramsay suggests that since the misfit his model leads to is less for larger limb-length to layer-thickness ratios, such limb lengths will, in fact, be established, a value of at least 10:1 being suggested. In fact, the pattern of folds is established by some process such as buckling or the intersection of kink bands, the details of which are dependent upon the rheological properties, conditions of deformation, and the initial configuration (Pfaff and Johnson, 1989).

Does Ramsay's evolutionary model 'explain' the considered phenomena? It would seem that an explanation must rather lie in the determination, within a description of the process of folding, of the physical circumstances and conditions that determine these. Such an analysis leads to a model for both the initiation and evolution of fold form and determines the internal motions of the layers and the strain distribution within them. If the model does not fit all observations, one may modify it to close the gap.

2.3. Deformation within the layers: Ramsay's kinematic mechanism

To further "...try to discover the functions that might express their evolutionary development," Ramsay proposed a kinematic mechanism from which the internal deformation of the layers and the interfacial slip may be computed. One motivation for this is that it appears to lead to an explanation for the 'lock-up' of chevron folds at a limb dip of approximately 60°. Another motivation is to obtain the completeness of description seen in a mechanical model.

The kinematic mechanism is uniform, layer-parallel shear. Shearing must take place so that the transition between the straight portion of the layer and the curved hinge sectors is maintained, with continuity at the hinges. While the evolutionary model is based, in part, on such continuity, it does not require a description of how this is accomplished. The constraint at the hinge leads to the imposition of uniform shear along the limbs, far from the hinges relative to layer thickness (Bayly, 1976).

Such kinematic mechanisms are commonly related to the *constitution* of the deforming material. However, they are not constitutive relations because there is no connection implied or explicit, between stress and rate of deformation. If the considered material is layered rock, shear parallel to layering, or normal to it, as in kinking, is related to the 'weakness' of interfaces or soft interbeds relative to the 'strength' or 'competence' of stiff layers. The use of layer-parallel shear within the layers is problematic because nothing in the appearance or likely constitutive behavior of the stiff layers would make this mechanism probable as the dominant mode of deformation (Bayly, 1976). Moreover the proposed kinematic mechanism does not simulate the observed strain related to bending in the hinges (see Fig. 5a). If one could refer to mechanics—and, again, no formal procedure for doing so is available—the implied jump in shear stress along the axial surface would violate the condition of stress equilibrium. Bayly (1976) makes much the same observations in a comment on Ramsay's paper.

The change in bulk shear with bulk shortening, $d\gamma/d\varepsilon$, is considered significant for this kinematic model, and certain conclusions are drawn from its variation with limb dip. Since $\gamma = \tan\theta$, Eq. (3) gives

$$d\gamma/d\theta = [-(1 - \nu\theta)\sin\theta\cos^2\theta]^{-1} \quad (7)$$

and Eq. (1) can be used to relate ε to θ. From these relations $-d\gamma/d\varepsilon$ vs -100ε may be computed, as in Ramsay (1974, fig. 2). Since Eq. (7) is infinite at $\varepsilon = 0$, so is $-d\gamma/d\varepsilon$. For small ν, this quantity has a minimum at $\varepsilon = -0.18$ (18% shortening) and a limb dip $\theta = 35°$, and then increases sharply in the range of 60–70% shortening, or $\theta = 66$–$72°$.

From this behavior, Ramsay (1974) draws the following conclusions. "Inside the competent layers, the rates of shear strain are very high at the start of folding and subsequently decrease. There is, therefore, a critical threshold that must be overcome before folding of the chevron style can begin to develop. For any compressive stress deviator acting along the layer, the threshold is a function of dip; certain minimum dip values must be attained (probably by buckling instability) before folding goes on in the manner suggested by the model analysis. The threshold of folding is also controlled by the internal flow properties of the competent layers and is not dependent upon the frictional effects along surfaces separating the competent layers."

These remarks, while seemingly based on mechanical principles, make no appeal to them explicitly. Buckling involves layer-parallel shortening, is strongly sensitive to the interfacial conditions, and involves negligible,

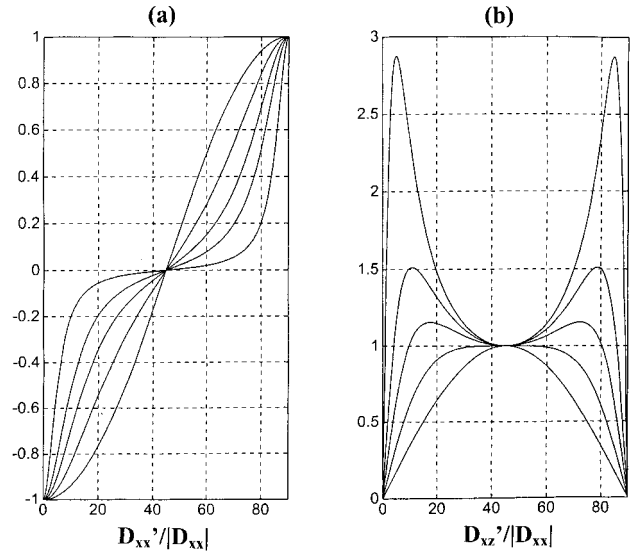

Fig. 2. Rates of (a) layer-parallel shortening or extension and (b) layer-parallel shear for the anisotropic medium model as a function of limb dip, for m = 1, 2, 4, 8, and 32.

rather than large, layer-parallel shear (see Fig. 5). While a transition between sinusoidal and chevron fold form occurs, nothing usefully described as a 'critical threshold' is involved. The kinematic model does not describe fold initiation or the transition from sinusoidal to chevron form. At $\theta = 0$, which the model identifies with $\varepsilon = 0$, no amount of layer-parallel slip or shear will lead to bulk shortening. This is the only meaning of the infinity in $d\gamma/d\varepsilon$.

The low values of $-d\gamma/d\varepsilon$ at intermediate limb dip are associated with the 'ease of formation of the folds,' whereas large values at large limb dip are associated with 'lock-up' of chevron folds (Ramsay, 1974, p. 1742, points 2 and 3). Again, no explicit relation defines 'ease of folding,' which might presumably be tied to the operative stress. Ramsay's ideas appear to derive from an assumption of frictional behavior, but an increase in $-d\gamma/d\varepsilon$ has no bearing on this, since, in simple frictional behavior, the rate of slip is irrelevant. In the viscous model (see Fig. 2), 'lock-up' does not occur.

An attempted link is often made, as here, between results for an ad hoc kinematic model, in which physics plays no part, and intuitive ideas as to process. However plausible these may seem, they provide no substantive basis for further investigation because the relevant physical quantities (stress, constitutive properties, friction) are absent in the ad hoc model. The mechanical modeling described below shows how the transition from sinusoidal to chevron folding takes place and provides a detailed picture of the kinematics, evolution, and fold form. Each of the two models is set up by a choice of constitutive relations and boundary and initial conditions.

3. Mechanical model for chevron folds

3.1. Equivalent anisotropic medium

A mechanical analysis of chevron folds has been based on the constitutive relations for a finely layered composite (Bayly, 1964). With further development, this approach leads to a complete approximate theory (Biot, 1965a,b; Cobbold, 1976; Casey and Huggenberger, 1985), in which only the effects of finite layer thickness and the details of behavior in the fold hinges are missing.

Bayly (1964) considers the alternation of two layer types of different thickness and viscosity. Because spatial variation in behavior along the fold limb is ignored, it may be represented by that in an anisotropic viscous fluid, characterized by a viscosity η_n in shortening or extension parallel to layers, respectively, and a viscosity η_s in shear. Bayly (see also Chapple and Spang, 1974) gives expressions for these viscosities for a composite of alternating layers. In the present case, we take the interfacial slip rate proportional to the resolved shear stress. If x′ and z′ denote directions parallel and normal to the layers, respectively, the slip velocity for a single interface is

$$\Delta\{u'\} = \beta\sigma_{xz}'. \tag{8}$$

Expressed as a shear rate added to the shear across the layer whose viscosity is η, we have for the bulk rate of shear

$$D_{xz}' = [(1/2\eta) + \beta/2H]\sigma_{xz}' = (1/2\eta_s)\sigma_{xz}'. \tag{9a}$$

The rate of layer-parallel shortening or extension is

$$D_{xx}' = (1/2\eta)(\sigma_{xx}' - \sigma_{zz}') = (1/2\eta_n)(\sigma_{xx}' - \sigma_{zz}'). \tag{9b}$$

The ratio of viscosities

$$m = \eta_n/\eta_s = 1 + \beta\eta/H = 1 + 1/\omega^* \tag{10}$$

where m is the strength of anisotropy, plays an important role in the subsequent analysis. The slip parameter, ω^*, enters into results given later for the discrete multilayer.

If axes x and y are parallel to the direction of shortening and parallel to the axial planes, tensor transformation yields, from Eqs. (9a) and (9b)

$$\begin{aligned} 2\eta_n D_{xx} &= (\cos^2 2\theta + m\sin^2 2\theta)(\sigma_{xx} - \sigma_{zz})/2 \\ &\quad - (m-1)\cos 2\theta \sin 2\theta \sigma_{xz} \\ 2\eta_n D_{xz} &= -(m-1)\cos 2\theta \sin 2\theta(\sigma_{xx} - \sigma_{zz})/2 \\ &\quad + (\sin^2 2\theta + m\cos^2 2\theta]\sigma_{xz}. \end{aligned} \tag{11}$$

If a symmetric pair of limbs undergoes shortening normal to the axial plane at a rate D_{xx}, the shear stress on the axial plane, σ_{xz}, vanishes. The relations Eq. (11) then yield

$$D_{xz} = -(m-1)\cos2\theta\sin2\theta(\cos^2 2\theta + m\sin^2 2\theta)^{-1} D_{xx}. \quad (12)$$

Transforming back to the components referred to coordinates x′ and y′, the rates of shear and shortening or extension along the layers are, for a left-dipping limb,

$$D'_{xz} = -m\sin2\theta D_{xx}/(\cos^2 2\theta + m\sin^2 2\theta) \quad (13a)$$

$$D'_{xx} = \cos2\theta D_{xx}/(\cos^2 2\theta + m\sin^2 2\theta). \quad (13b)$$

A relationship equivalent to total shear in the limb, $-d\gamma_\Sigma/d\varepsilon$, can be derived from Eqs. (13a) and (13b), since

$$-d\gamma_\Sigma/d\varepsilon = -(d\gamma_\Sigma/dt)/(d\varepsilon/dt) = -2D'_{xz}/[(1+\varepsilon)D_{xx}]. \quad (13c)$$

Comments on this quantity were made earlier. Since, by Eqs. (13a) and (13b), $-d\gamma_\Sigma/d\varepsilon$ only relates to layer-parallel shear and interfacial slip, it is unlikely to provide by itself much insight into the folding process. We accordingly turn to a direct treatment.

For a straight-limbed chevron fold, Eqs. (13a) and (13b) suffice to describe its evolution. By consideration of the geometry (Bayly, 1964; Cobbold, 1976; Bayly and Cobbold, 1979):

$$d(\tan\theta)/dt = -2\{\tan\theta + (m-1)\sin2\theta\cos2\theta/[\cos^2 2\theta + m\sin^2 2\theta]\}D_{xx}. \quad (14)$$

From Eq. (14) we may compute the evolution in the dip of the fold with bulk shortening. Since, for $\theta = 0$, the right-hand side of Eq. (14) vanishes, some initial dip is required for folding to occur. The relation between bulk shortening and dip depends on initial dip (see Bayly, 1964). Layer-parallel shortening is significant at low limb-dip, and depends upon the strength of anisotropy, m (Fig. 2). Above a dip of 45°, the layer undergoes a superposed extension [Eqs. (13a) and (13b) and Fig. 2]. These features are not present in the ad hoc evolutionary model. The deviatoric stress needed to maintain the rate of bulk shortening (Fig. 3) is

$$-(\sigma_{xx} - \sigma_{zz}) = 2\eta_n D_{xx}(\cos^2 2\theta + m\sin^2 2\theta)^{-1}. \quad (15)$$

Tightening of the fold may be kept track of either by the limb dip, θ, or by its tangent, as a function of some measure of the bulk shortening (see Cobbold, 1976). An easily visualized measure is the ratio of the span of the fold limb to its initial value, $X/X_0 = \exp(D_{xx}t)$. An initial dip is specified at $X = X_0$. Limb dip as a function of X/X_0 is shown in Fig. 4(a) for an initial dip of 1° and for the values m = 1, 2, 4, 8, 16, and 128. For the isotropic fluid, m = 1, the amplification is purely kinematic (here, a term in mechanics corresponding in this case roughly to 'passive folding').

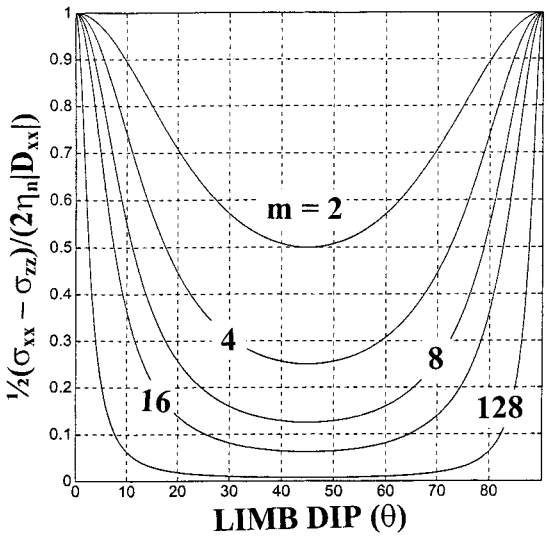

Fig. 3. Applied deviatoric stress, $[(\sigma_{xx}-\sigma_{zz})/2]/(2\eta_n D_{xx})$, required for straight-limbed folding in the anisotropic viscous fluid, as a function of limb dip, θ, for m = 1, 2, 4, 8, 16 and 128. The Ramsay model is, in a sense, approached when m is very large, in which case the stress level remains low for limb dips well beyond values suggested for lock-up.

The rate of growth in slope, $d\theta/d\tau$, in radians, where $\tau = |D_{xx}|t$, vs dip (Fig. 4b) more clearly distinguishes qualitatively different phases in fold growth. Two sets of curves are shown for m = 1, 2, and 8. The curves meeting at 45° are the exact expressions obtained from Eq. (14). Beyond 45° all curves fall with little difference between them. The other curves approximate Eq. (14) to terms $\sim\theta^3$. The approximation is adequate over a portion of the period of rapid growth, but does not accurately capture the magnitude or position of the maximum rate of amplification or the later behavior. A corresponding approximation for a viscous multilayer may also be obtained. It will have the same deficiencies, but both provide a good description of the sinusoidal-to-chevron transition (the result for the viscous multilayer is given later).

Fig. 3 gives the variation in the driving deviatoric stress, Eq. (15), normalized by $2\eta_n|D_{xx}|$, with limb dip for m = 1, 2, 4, 8, 16, and 128. The minimum value at 45° is $1/m$; the breadth of the region of minimal stress increases with m. As Ramsay (1974) notes, in the case

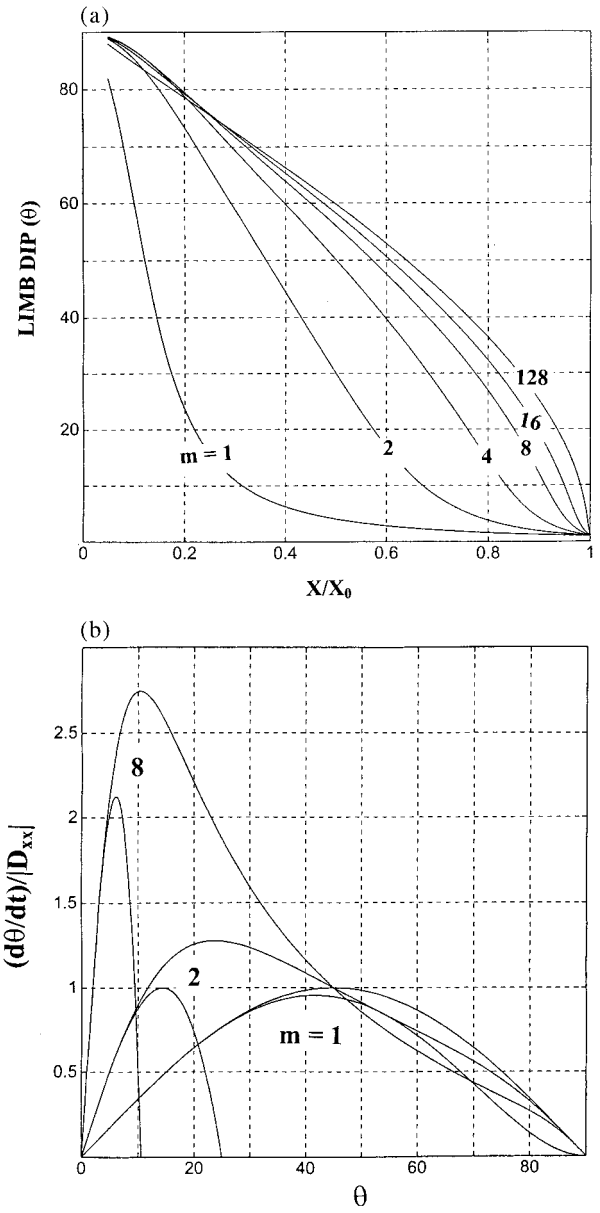

Fig. 4. (a) Evolution of the dip of a fold limb with an initial dip of 1° vs shortening measured by the current to initial span of the limb normal to the axial plane, X/X_0, for m = 1, 2, 4, 8, 16 and 128. The result for the isotropic medium, m = 1, is just the kinematic or passive amplification. (b) The rate of change in dip, $d\theta/dt$, normalized by the bulk rate of shortening, $|D_{xx}|$, as a function of dip, for m = 1, 2 and 8. The upper curves are the exact result; the curves coinciding with these at low limb dip are expansions to third-order terms in the tangent of the dip angle. Near coincidence of the curves defines the range in which approximations to this order are likely to give good results for other quantities, as in those illustrated in Figs. 5 and 6.

of alternating stiff and soft layers that behave in a viscous manner, the notion of fold 'lock-up' does not apply. Fig. 2 shows the rates of layer-parallel shortening or extension and of layer-parallel shear as functions of limb dip for m = 1, 2, 4, 8, and 32. For m = 32, appreciable shortening only occurs through the first 10° of dip and appreciable extension only after 80°; the latter is not likely realized in most natural cases.

A restriction of the analysis to straight-limbed folds need not apply (Cobbold, 1976; Casey and Huggenberger, 1985). For symmetric folds of arbitrary form undergoing shortening normal to the axial planes, Eq. (14) is the material time derivative of the tangent of the local dip angle and the rate of shortening, D_{xx}, is uniform across the fold. The evolution equation for the fold form is then

$$\mathrm{D}(\tan\theta)/\mathrm{D}t = \partial(\tan\theta)/\partial t + D_{xx}x\partial(\tan\theta)/\partial x \tag{16}$$

where this quantity is given by Eq. (14). The result of Eq. (16) allows us to follow the transition between an initial sinusoidal form to a chevron form. These forms may be represented by a trace parallel to the layering with height above its mean level (see also Hudleston, 1973).

$$\zeta(x,t) = A\cos(\lambda x) + A''\cos(3\lambda x). \tag{17}$$

The amplitudes A, A'' and the wavenumber $\lambda = 2\pi/L$, where L is the wavelength, are functions of time; $\lambda(t) = \lambda(0)\exp(D_{xx}t)$. Since $\tan\theta = \mathrm{d}\zeta/\mathrm{d}x$, Eqs. (14) and (16) provide the evolution equations for A and A''

$$\mathrm{d}A/\mathrm{d}t = [q_{11}A + q_{13}(\lambda A)^2 A]D_{xx}$$

$$\mathrm{d}A''/\mathrm{d}t = [q_{33}A'' + q_{31}(\lambda A)^2 A]D_{xx}. \tag{18a}$$

For the anisotropic medium:

$$q_{11} = q_{33} = 4(m-1) + 1$$

$$q_{13} = -(4m^2 - 5m + 1)$$

$$\text{and } q_{31} = (1/3)(4m^2 - 5m + 1). \tag{18b}$$

Integration of Eqs. (18a) and (18b) to the same order of approximation yields

$$A(\tau) = A_0\{\exp(q_{11}\tau) - (q_{13}/2q_{11})(\lambda A_0)^2[\exp(q_{11}\tau) - \exp(3q_{11}\tau)]\}$$

$$A''(\tau) = A_0[q_{31}/(3q_{11} - q_{33})](\lambda A_0)^2[\exp(q_{11}\tau) - \exp(3q_{11}\tau)] \tag{19}$$

where $A_0 = A(0)$, $A''(0) = 0$, and $\tau = |D_{xx}|t$.

The transition between the sinusoidal and chevron forms is recorded in the value of the amplitude ratio A''/A. At the dip at which the approximation breaks down for the value m = 8 in the anisotropic medium (Fig. 4b) and for an initial dip of 1°, $\theta = 6.6°$ at

$X/X_0 = 0.85$, the ratio is $A''/A = 0.054$. In an ideal chevron form, $A''/A = 1/9 = 0.111$ (Hudleston, 1973). Thus, even at this low limb dip the fold for this case has a strong chevron character.

We have computed results to terms $\sim\theta^3$ for the symmetric folding of a viscous multilayer by means of the method described in Johnson and Fletcher (1994), for which the anisotropic fluid serves as an approximations, to study the effect of finite-limb-length to thickness ratio, $(L/2)/H$. The ease of slip on the interfaces is assigned to be equivalent to the above case, $m = 8$. For $(L/2)/H = 5$, at $\theta = 7.8^\circ$ and $X/X_0 = 0.73$, $A''/A = 0.013$, indicating a much less straight-limbed structure. For $(L/2)/H = 10$, at $\theta = 6.3^\circ$ and $X/X_0 = 0.82$, $A''/A = 0.020$; and for $(L/2)/H = 40$, at $\theta = 5.8^\circ$ and $X/X_0 = 0.86$, $A''/A = 0.050$. Thus, for the multilayer, the transition to chevron form is well underway at low limb dip, even for a modest degree of anisotropy, provided the limb length to thickness ratio is relatively large. In the multilayer, rounding at the hinges will always be present at the scale of the layer thickness.

3.2. Viscous multilayer and deformation within a layer

The approximate solution for the viscous multilayer also provides the components of stress and rate of deformation within the layer and the rate of interfacial slip. These results conform qualitatively to observations of strain and fold form in the hinge regions of some natural folds (Chapple and Spang, 1974). They provide a basis for comparison with Ramsay's kinematic model.

The normal rate of deformation, D_{xx}, is no longer uniform; its mean or basic-state value is denoted by an overbar, $\bar{D}_{xx}$. For the small dip in the example, it suffices to show the results for D_{xx} and D_{xz}, rather than

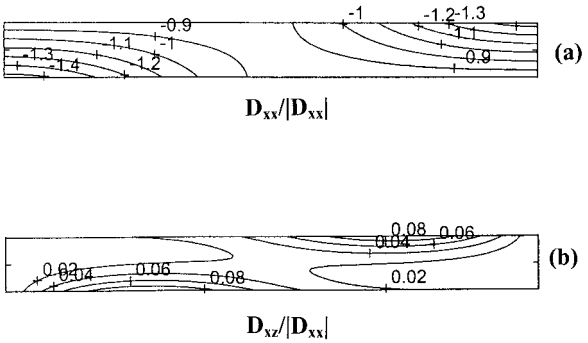

Fig. 5. Distribution of the rate of deformation components (a), D_{xx}, and (b), D_{xz}, normalized by the absolute value of the bulk rate of shortening, $|\overline{D_{xx}}|$ in the left-dipping limb of a symmetric viscous multilayer fold, as obtained from the third-order analysis. Parameters are $(L/2)/H = 10$, dip $\theta = 6^\circ$, and slip parameter $\omega^* = 1/7$, corresponding to an effective viscosity ratio $m = 8$. See text for further discussion.

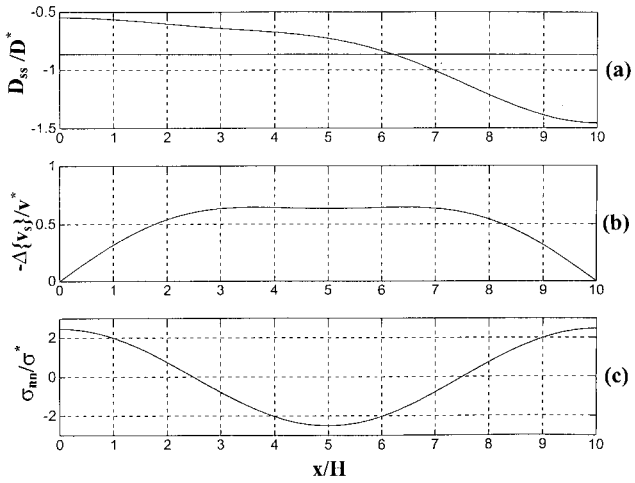

Fig. 6. Distribution of (a) the tangential normal stress, D_{ss}, (b) the rate of interfacial slip, $\Delta\{v_s\}$, and (c) the variable part of the normal stress, all on the upper surface of the layer, for the same case as in Fig. 5. The normalizing quantities are $D^* = |\bar{D}_{xx}|$, $v^* = H|\bar{D}_{xx}|$, and $\sigma^* = 2\eta_n|\bar{D}_{xx}|$.

for components referred to axes parallel and normal to layering.

The spatial distribution of the component D_{xx} shows three effects (Fig. 5a). The most prominent feature is an increase (lower negative value) in the external portion of the hinge and a decrease (greater negative value) in the internal hinge region. This corresponds to bending superposed on uniform layer-parallel shortening with the normalized basic-state value of -1. Second, there is a noticeable reduction in the rate of shortening along the limbs, and a corresponding mean increase at the hinges. Third, there is a pronounced asymmetry, with greater concentration of shortening in the internal hinge region. This last effect is also shown by the distribution of the interface-parallel rate of deformation, D_{ss} (Fig. 6a).

The rate of layer-parallel shear, D_{xz}, within the layer is small (Fig. 5b). An estimate of the partitioning of bulk layer-parallel shear between that internal to the layer and that from interfacial slip from Eq. (9a) is

$$[\Delta\{v_s\}/H]/[\sigma'_{xz}/2\eta] = 1/\omega^* \tag{20}$$

where v_s is the velocity component locally tangent to the interface. With increasing dip, the distribution of $\Delta\{v_s\}$ goes from one that is sinusoidal along the limb to one that is nearly uniform along the bulk of the limb and falls off steeply in the hinge regions (Fig. 6b).

In the mechanical analyses discussed here, layers are incompressible and voids cannot open along the hinges. Generalization to include hinge dilation is possible. Dilation might involve diffusive transport of material from the fold limbs or from the layer's strongly compressed internal hinge region itself. Flow of soft interbeds towards the hinge has been proposed

(Williams, 1980). These mechanisms maintain constant cross-sectional area. An opening may be created and filled either by fluid or solid material transported from a more distant source. The tendency for such effects is indicated by the normal stress distribution along a layer interface (Fig. 6c, see also Cobbold, 1976). The variable part of the normal stress is very large for such a low limb dip with tension concentrated across the hinge. This would lead to flow of any weak interbed material, or to the diffusive transport of soluble phases, or may, in concert with pore fluid pressure, result in interfacial fracture and opening of a void space. A portion of a layer near the hinge may act like a free plate, built in away from the hinge. If this portion is long enough, it may undergo localized buckling, providing a mechanism for producing a bulbous hinge structure. Cobbold (1976) gives a result of this type on the normal stress in an anisotropic medium, and points out its bearing upon metamorphic differentiation by limb dissolution and hinge precipitation. Gray and Durney (1979, see their fig. 2 and discussion in text) have carried out an analysis of such differentiation for the multilayer case.

4. Summary—chevron folds

Geometric, evolutionary, and kinematic models for chevron folds and chevron folding provide a fruitful subject for critical discussion. While these models distill much experience from the field examination of folds, a field study informed by mechanical analysis of simple models would involve other quantitative observations. As anticipated, the geometric model approximates folds seen in nature, especially when the flow of soft interbeds or development of saddle reefs leads to a nearly uniform thickness of the stiff layers through their hinges. The evolutionary model does not accommodate layers of unequal thickness, and explanatory power is attributed to this fact for observed features of natural chevron folds. However, we contend that this explanation can only be provided through the explicit cause and effect constructs of a complete mechanical model. An essential feature of such a procedure is that such a model may fail to produce observed features; it is accordingly refutable.

Mechanical modeling of the early stages of folding in an anisotropic viscous medium or viscous multilayer with interfacial slip shows a transition between sinusoidal and chevron forms (for finite amplitude simulations see Casey and Huggenberger, 1985; Cobbold, 1976). Deformation within the layers of the multilayer is in good accord with observation. It is clear that satisfactory models for natural chevron folds could be further pursued by this methodology, introducing refinements in the areas of constitutive behavior, and a treatment of a sequence with unequally thick layers. Such models would provide a sound basis for interpreting all quantitative data from natural folds, including systematic discrepancies from idealized geometry.

The failure of Ramsay's kinematic model is at least one example of the inability to make sense of a process of deformation, despite a great deal of observational experience in the field, without a working knowledge of a complete mechanics. We would contend that this example is not an exception and offer a second example to further illustrate this point.

5. Two mechanisms for échelon vein formation

The laboratory experiments of Riedel (1929) and Cloos (1955) illustrated one possible mechanism for the formation of échelon vein segments: when a clay cake was deformed by sliding one underlying board past another, simulating a narrow strike-slip fault at depth, a broader zone of shearing and fracturing developed within the clay cake. When the upper surface of the clay cake was wet, opening fractures appeared there, oriented about 45° from the trend of the shear zone. With further shearing, the central part of the fractures rotated to greater angles, while propagation continued at the fracture tips in the 45° direction. This mechanism created échelon fractures with sigmoidal shapes. These fractures in clay have been used as possible analogs for échelon vein segments in rock, and their development has been described in terms of a kinematic model based on simple shearing deformation (Ramsay, 1967).

Laboratory experiments by Sommer (1969) illustrated another possible mechanism for échelon vein formation. Sommer loaded glass rods in tension until an opening fracture developed on a diametral plane. Then a torque was added to the applied load to introduce a spatial rotation of the principal stress trajectories about the radial direction, parallel to fracture propagation. In the terminology of fracture mechanics (Lawn and Wilshaw, 1975), this corresponds to a mixture of mode I loading (opening) and mode III loading (shearing parallel to the fracture tip). With further propagation the parent fracture broke down into an array of échelon partial fractures with surfaces that twist about an axis parallel to the propagation direction. These partial fractures have been used as possible analogs for échelon vein segments (Pollard et al., 1982).

5.1. Nature and cause of debates about échelon vein formation

Since these early experiments numerous structural geologists, including Shainin (1950), Wilson (1952),

Roering (1968), Lajtai (1969), Hancock (1972), Beach (1975), Knipe and White (1979), Ramsay (1980), Rickard and Rixon (1983), Ramsay and Huber (1983, pp. 23–26 and 48–52), Nicholson and Pollard (1985), Granier (1985), Collins and De Paor (1986), Engelder (1987), Nicholson and Ejiofor (1987), Ramsay and Huber (1987, pp. 595–640), Shaoxun and Xiaoshuang (1988), Craddock and van der Pluijm (1988), Rothery (1988), Olson and Pollard (1989), and Smith (1995), have described and interpreted échelon vein segments, some with sigmoidal shapes, and some forming conjugate arrays.

A number of debates have arisen in this literature. For example, are the vein segments 'tensile' or 'shear' in origin? That is, do they form perpendicular to the least compressive (most tensile) stress, or on planes oriented oblique to the principal stress directions that carry significant resolved shear stress? Do the segments predate and serve to localize the shearing deformation along the array, or does the zone of shearing predate and serve to localize the development of the fractures? Does the angle, δ, between the trend of the array and the trend of individual segments enable one to distinguish tensile origins (extension fractures form at $\delta = 40^\circ$–45°) from shear origins (Riedel shears form at $\delta = 10^\circ$–20°), or does it distinguish volumetric increase (positive dilation produces arrays with $\delta < 45^\circ$) from volumetric decrease (negative dilation produces arrays with $\delta > 45^\circ$) as superimposed on simple shear deformation ($\delta = 45^\circ$)? Is the sigmoidal shape of vein segments diagnostic of rotation within a shear zone, or of a curved fracture propagation path caused by mechanical interaction of two adjacent opening fractures?

There seems little doubt that the two mechanisms mentioned above can produce échelon vein segments, but the debates continue about interpretation methods, and diagnostic criteria are poorly understood. Here we ask: Why does this uncertainty concerning the interpretation of échelon veins persist, given the fact that the original concepts stemming from the experiments of Riedel (1929) and Sommer (1969) are now 70 and 30 years old, respectively? Are the problems intractable? We doubt it. Are the problems unimportant? The volume of literature attests to the importance attributed to these structures by structural geologists. Rather, we suggest that the lack of progress can be attributed to the inadequate methodology used by structural geologists to address the origins of these structures. Furthermore, we propose that a methodology based on a complete application of continuum mechanics would provide the understanding and the diagnostic tools for interpreting échelon veins.

Because different physical mechanisms can apparently result in similarly shaped vein segments, interpretations based only on the magnitude of vein-array angles or the angle between conjugate arrays are likely to be problematic. Limiting an analysis to considerations of kinematic quantities and ignoring the role of stresses and the necessity for mechanical equilibrium, as well as the specific constitutive relationships describing material behavior, is likely to be inadequate. Most of the studies cited above involve interpretations of échelon veins in the context of a homogeneous strain field (e.g. using Mohr circles for strain) or a homogeneous stress field (e.g. using Mohr–Coulomb failure envelopes). However, once a vein segment has initiated, such a context is necessarily inappropriate because the discontinuity in displacements across a vein segment produces a strongly heterogeneous local strain and stress field.

In an article published in 1991 in the *Journal of Structural Geology*, a different approach for investigating and interpreting échelon vein arrays was advocated (Olson and Pollard, 1991). The authors suggested that future interpretations utilize solutions for the appropriate boundary and initial value problems of continuum mechanics. These solutions are not limited to consideration of strain or rate of deformation. Rather, they incorporate all the mechanical quantities of interest and they are based on explicit relationships among these quantities derived from fundamental principles (e.g. conservation of mass, momentum, and energy). Furthermore, these solutions employ specific constitutive relationships, rather than an appeal to brittle vs ductile behavior. For example, if the veins formed in an elastic rock, the stress tensor is related to the infinitesimal strain tensor through Hooke's Law (Timoshenko and Goddier, 1970). If the veins formed in a rock undergoing viscous flow, the stress tensor and pressure are related to the rate of deformation tensor through Stokes' equations (White, 1974). More complex constitutive laws (e.g. viscoelastic or plastic) can be employed if the elementary laws prove inadequate or if laboratory data suggest such laws are warranted. This is what we mean by a complete mechanics.

6. Heterogeneous strain fields associated with échelon veins

To illustrate a possible heterogeneous strain field associated with the opening of échelon vein segments, we consider a model of échelon crack growth in a linear elastic body. The region of interest has a cross-sectional area of 1 m^2 and an initial array of five flaws (short cracks) with lengths of 1 cm, spacings of 5 cm, and a flaw-array angle $\delta = 50^\circ$. During the numerical experiment these flaws grow into sigmoidal cracks with lengths of about 8 cm (Fig. 7). The constitutive properties of the elastic material are Young's modulus, $E = 60$ GPa, and Poisson's ratio, $\nu = 0.25$ (Clark,

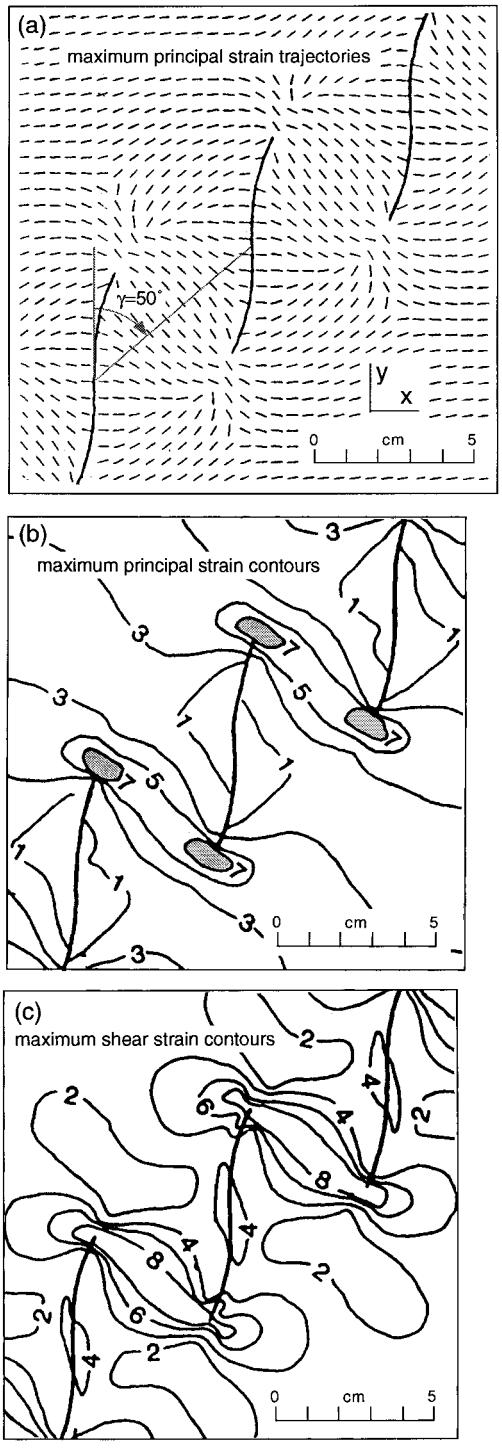

Fig. 7. Different components of the heterogeneous strain field near a set of five échelon cracks. (a) Trajectories of the maximum principal strain, ε_1. (b) Contoured magnitudes of ε_1 multiplied by 10^4. (c) Magnitudes of the maximum shear strain, γ_{max} multiplied by 10^4.

1966), and the fracture toughness is $K_{IC} = 2.7$ MPa $m^{1/2}$ (Atkinson and Meredith, 1987). This numerical model experiment is described more fully in Olson and Pollard (1991), but certain aspects of the strain field near the three central cracks are shown in Fig. 7(a–c).

The boundary conditions before propagation of the cracks consist of remote stresses, σ_{ij}^r, and stresses acting on elements adjacent to the crack surfaces, σ_{ij}^c, defined by the components:

$$\sigma_{xx}^r = -p,\ \sigma_{xy}^r = 0,\ \sigma_{yy}^r = -p \text{ in the remote field;}$$

$$\sigma_{xx}^c = -p,\ \sigma_{xy}^c = 0 \text{ on the crack surface.} \quad (21)$$

The magnitude of the internal fluid pressure, p, is equal to the remote isotropic normal compressive stress.

To initiate crack growth a displacement of 1.55×10^{-2} cm is imposed on the left- and right-hand edges of the body in the x-coordinate direction, and the top and bottom edges are not allowed to displace in y. Thus, the remote components of infinitesimal strain induced by these displacements are:

$$\varepsilon_{xx}^r = \varepsilon_1^r = 3.1 \times 10^{-4},\ \varepsilon_{yy}^r = \varepsilon_2^r = 0. \quad (22a)$$

These components are the principal strains. The remote maximum shear strain induced by these displacements is:

$$\gamma_{max}^r = (\varepsilon_1^r - \varepsilon_2^r) = 3.1 \times 10^{-4}. \quad (22b)$$

This is the shear strain associated with material lines at 45° to the coordinate axes, and therefore it is approximately the remote shear strain parallel to the array of cracks. These strain components would be homogeneously distributed throughout the body in absence of any cracks: the cracks perturb this strain field as illustrated in Fig. 7.

The stress intensity factors at the flaw tips in the initial state are about $K_I = 2.76$ MPa $m^{1/2}$, just sufficient to exceed the fracture toughness and cause propagation. The flaws start to propagate in the y-coordinate direction, perpendicular to the remote least compressive stress (applied extension), until significant mechanical interaction with neighboring cracks diverts their paths into sigmoidal traces directed toward their neighbors (Fig. 7a). As the cracks propagate, a strain field develops in the elastic body that is non-homogeneous in both space and time. Each increment of crack propagation is prescribed to be perpendicular to the local maximum tensile stress (maximum extensional strain, ε_1) just ahead of the fracture tip (Thomas and Pollard, 1993). In Fig. 7(a) the direction of ε_1 throughout the field of view is indicated by the tic marks. The magnitude of ε_1 is contoured in Fig. 7(b) where the shaded regions mark the strain concentrations associated with the crack tips.

Because the conditions of crack growth are known in this experiment, we can say with certainty that the remote principal strain and stress orientations are recorded by the orientations of crack surfaces near their middles, but not near their tips. There, the mechanical interaction with neighbors produces crack surfaces that are not perpendicular to the remote least compressive stress (maximum extensional strain).

An estimate of the average strain accommodated by vein opening is given by the segment aspect ratio, the ratio of opening displacement discontinuity to segment length. For dominantly elastic deformation this aspect ratio should not exceed laboratory strains associated with the onset of inelastic deformation, typically less than a few percent (Jaeger and Cook, 1969). Some vein segments have such small aspect ratios (Ramsay and Huber, 1983, p. 51, fig. 3.22A); other vein segments are observed with aspect ratios as great as 10% (Ramsay and Huber, 1983, p. 51, fig. 3.22B), suggesting that the material properties during growth of these veins was, in part, inelastic. Such veins require a different constitutive law from the one employed above. For example, one might turn to solutions for fracture growth in dilatant materials (Casey, 1980), or in viscoelastic materials (Kanninen and Popelar, 1985).

6.1. Possible errors introduced when using a kinematic model

According to the most elementary kinematic model (Ramsay, 1967, pp. 88–91), vein segments form during the initial increment of deformation in a zone of homogeneous simple shearing and are oriented perpendicular to the maximum extension, that is at an angle, $\alpha = 45^\circ$ to the shear zone. The shear strain is related to the rotation of a material line element within the zone as (Ramsay and Huber, 1983, p. 24):

$$\gamma = \cot\alpha - \cot\alpha' \tag{23a}$$

where α is the initial angle between the line element and the shear zone boundary, and α' is the final angle of the rotated line element. In this context the central part of a vein segment is assumed to behave like a material line element and therefore to rotate during shearing according to Eq. (23a).

To quantitatively assess the possible errors introduced by using this kinematic model, we apply it to the sigmoidal échelon cracks illustrated in Fig. 7. We use this array because we know the actual kinematics. From the geometry of the cracks alone (Fig. 8), the shear zone boundaries are interpreted to trend at an angle of 50° to the central part of the cracks. These parts are interpreted to have rotated from $\alpha = 45^\circ$ to $\alpha' = 50^\circ$, so the shear strain is:

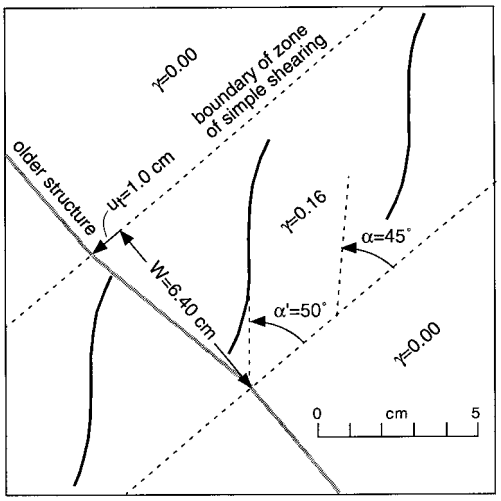

Fig. 8. Interpretation of the échelon crack array shown in Fig. 7 using a simple shear kinematic model. The estimated homogeneous shear strain, γ, is 0.16 inside the shear zone and zero outside the zone.

$$\gamma = \cot 45^\circ - \cot 50^\circ = 1.6 \times 10^{-1}. \tag{23b}$$

Thus, using the kinematic model, one would interpret the échelon crack segments in Fig. 8 as lying in a shear zone with about 16% shear strain.

The actual distribution of shear strain associated with these sigmoidal échelon cracks is shown in Fig. 7. Although it clearly is not homogeneous, we can compute the average shear strain across a zone of comparable width to that interpreted in Fig. 8, that is $W = 6.4$ cm. According to the solution to the elastic boundary value problem, the net tangential displacement across this zone is $u_t = 4.8 \times 10^{-3}$ cm. Thus, the average shear strain is:

$$\gamma = \frac{u_t}{W} = \frac{4.8 \times 10^{-3}\ \text{cm}}{6.4\ \text{cm}} = 7.5 \times 10^{-4}. \tag{24a}$$

The actual shear strain is over two orders of magnitude less than that calculated assuming homogeneous simple shear. It should be clear from this comparison that significant quantitative errors can result if a kinematic model is adopted for an échelon array that formed by fracture growth in an elastic rock.

A diagnostic criterion to distinguish sigmoidal vein segments formed by rotation in a shear zone is measurement of the net tangential displacement, u_t, across the zone. This displacement should be consistent with the magnitude of the shear strain inferred from the vein geometry. For the geometry shown in Fig. 8:

$$u_t = \gamma W = (1.6 \times 10^{-1})(6.4\ \text{cm}) = 1.0\ \text{cm}. \tag{24b}$$

Cross-cutting markers would be offset by about 1.0 cm across the 6.4 cm wide shear zone, compared to an off-

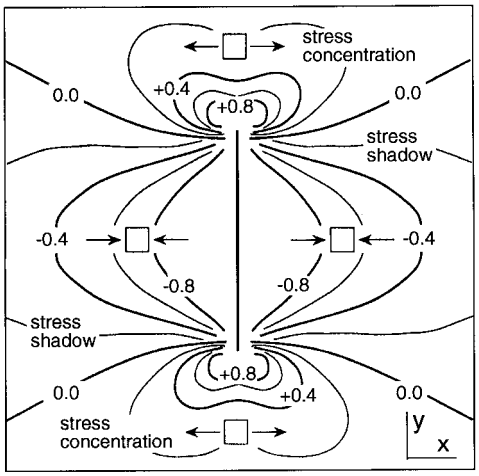

Fig. 9. Contours of the magnitude of the stress component σ_{xx}, the normal stress acting in the x-coordinate direction as induced by a uniform fluid pressure within a crack. A stress shadow is indicated by the negative (more compressive) values to each side of the crack, and a stress concentration by the positive (more tensile) values ahead of the crack tips.

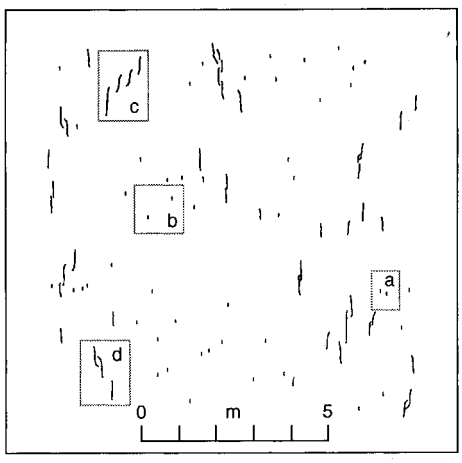

Fig. 10. Resulting crack pattern from a numerical experiment in which 100 randomly located flaws are loaded by a remote biaxial compressive stress and an internal fluid pressure such that they propagate. Mechanical interaction causes some to turn toward neighboring cracks forming sigmoidal échelon arrays. Boxed regions are referred to in the text.

set of only 4.8×10^{-3} cm due to crack opening and propagation in an elastic rock. Furthermore, one would expect aspect ratios on the order of 10% for vein segments in such a shear zone.

7. A third mechanism for échelon vein formation

As an example of the richness that accompanies the use of a complete mechanical analysis, we review a third mechanism for the formation of échelon vein arrays that was discovered during numerical experiments (Olson and Pollard, 1991). In the preceding discussion we illustrated the perturbed strain field near arrays of échelon cracks (Fig. 7a–c), but the model does not address the cause(s) behind the development of the array itself: the initial flaws were prescribed to be in an échelon geometry. Here we describe how the perturbed stress field in the vicinity of a single opening crack can provide an explanation for the échelon geometry itself.

The distribution of the normal stress component, σ_{xx}, near a single, fluid-pressurized fracture in an infinite elastic body is shown in Fig. 9 (Olson and Pollard, 1991). The uniform remote compressive stress is subtracted from the stress field so the contoured values are the stress perturbation resulting from the opening of the crack. The normal stress in the regions that extend in front of the crack tips is tensile with a local stress concentration around the tip. Here, growth of sub-parallel cracks would be enhanced. In contrast, in the regions to either side of the crack, σ_{xx} is compressive, defining a stress shadow in which the growth of sub-parallel cracks would be inhibited.

To examine the role of this stress perturbation on the generation of échelon arrays, Olson and Pollard (1991) considered a population of randomly located flaws in a two-dimensional elastic body, subject to plane strain conditions. They used a boundary-element computer code modified from Crouch and Starfield (1983) with a linear elastic fracture propagation criterion (Erdogan and Sih, 1963; Ingraffea, 1981). The length of the flaws was 0.1 m, and the area of the representative volume of rock was 100 m^2. The boundary conditions were:

$$\begin{aligned}
&\sigma^{r}_{xx} = -20 \text{ MPa}, \ \sigma^{r}_{xy} = 0 \text{ MPa},\\
&\sigma^{r}_{yy} = -21 \text{ MPa in the remote field;}\\
&\sigma^{c}_{xx} = -24.7 \text{ MPa}, \ \sigma^{c}_{xy} = 0 \text{ MPa on the crack surfaces.}
\end{aligned} \tag{25}$$

This state of stress is thought to be plausible for conditions at about 1 km depth. The maximum circumferential stress at the crack tips is used as a criterion for propagation (Erdogan and Sih, 1963) and the fracture toughness is taken as $K_{IC} = 1.9$ MPa $m^{1/2}$ (Atkinson and Meredith, 1987).

One of many fracture patterns developed with different random locations of flaws in these numerical experiments is shown in Fig. 10. Note how the mechanical interaction between closely spaced cracks in each other's stress shadow prevents growth (Fig. 10, area a) and how the lack of strong positive interaction for widely spaced échelon cracks did not promote propagation (Fig. 10, area b). In contrast, closely-spaced échelon flaws with relatively small vein-array angles did grow readily (Fig. 10, areas c,d).

The angular relationships between cracks and their arrays were generalized from 100 numerical experiments. Because the initial flaw distributions were random, a wide range of crack spacings and crack-array angles were present. Arrays with $\delta < 50^\circ$ were favored for growth relative to arrays with $\delta > 50^\circ$. For moderate vein-array angles ($\delta < 45^\circ$), 75–100% of the cracks propagated, whereas less than 30% propagated with $\delta > 70^\circ$. For those cases with $\delta < 55^\circ$, increasing spacing decreased the effects of mechanical interaction that promote propagation (Fig. 10).

The numerical experiments demonstrate that a viable mechanism for the formation of échelon vein arrays is *self organization* resulting from mechanical interaction of randomly located flaws. This mechanism is distinct from localization within a shear zone and from localization at the tip of a mixed mode I–III fracture. A diagnostic criterion distinguishing vein segments formed by the latter mechanism is their direct connection to the parent vein (Nicholson and Ejiofor, 1987). If such connections are found by serial sectioning the rock specimens, this would rule out the mechanism of self-organization.

8. Summary—échelon veins

Whereas many discussions of échelon veins deal only with kinematic models that omit the strain perturbations caused by vein opening, a complete mechanical model explicitly includes the vein segments and their heterogeneous fields of strain and stress. With a complete model (in the example included herein limited to linear elastic materials) one can reproduce commonly observed features, such as sigmoidal vein shape, shear displacements across veins, and échelon arrays. We suggest that complete models utilizing visco-elastic and/or plastic material properties would reproduce many of the features common to échelon vein segments in shear zones, such as large apertures relative to segment lengths.

The elastic models helped to identify a third mechanism for échelon vein formation that is compatible with the full range of vein-array angles reported in the literature ($\delta = 0^\circ$ to 55°), demonstrating that interpretive methods using this angle to discriminate a shear zone origin from an origin related to breakdown of a parent opening fracture are not diagnostic. Furthermore, these models show how échelon veins may be the precursor to, and not the result of, localized shear deformation.

9. Concluding remarks

Tens of millions of dollars have been spent for laboratory determination of the mechanical properties of rocks, but little use is made of the resulting knowledge of constitutive behavior in structural geology and tectonics. Much time and effort is spent in structural geology classes teaching an incomplete mechanics, in which concepts of stress and strain and loose or incomplete statements of material behavior, are set forth to little apparent purpose. As a consequence, fundamental laws such as conservation of momentum, and elementary principles such as continuity of traction and restrictions on velocity components at interfaces, are violated, ignored, or not taken advantage of in setting up structural and tectonic hypotheses. The imaginations of many structural geologists are limited to an appreciation only of motions such as those derived from a uniform velocity gradient tensor. In an effort to fit the natural world within such a conceptual basis, a plethora of special notions has been created, all of which are unnecessary and many of which lead to error.

The fields of deformation obtained from solutions to boundary and initial-value problems simulate essential aspects of the processes producing the structures we observe and map in the field. In geometrical and kinematical modeling, on the other hand, the causal connection between these structures and the conditions of loading and constitutive behavior of rocks is too often pre-empted by a specification of mechanically unrealizable motions whose only virtue is that they lead to approximations of structural form, or permit restoration. On the basis of these models, no connection to the underlying physical process can be made.

We have shown, in two examples, that mechanical analysis leads to a richer collection of results and the posing and answering of many questions relevant to process. These results may be carried into the field as a sound intuitive basis for observing and interpreting similar, and, often, apparently quite different structures (Fletcher and Pollard, 1981). Conversely, the effort to simulate geometry alone often forces incomplete and physically implausible interpretations of kinematics and process. While a complete mechanical analysis is, in some respects, more difficult to learn and requires more work in application, it provides testable hypotheses and refutable outcomes.

It is not plausible even to suppose, much less to demonstrate, that a methodology based upon geometric idealization of structures, and a procedure for creating a sequence of restored structures that stipulates the motions required, can be consistent with a methodology based upon a complete mechanics. We do not deny that the former methodology may address a legitimate question in structural geology, and one motivated by economic concerns. On the other hand, it cannot replace, or even contribute to, the latter methodology as a means of unraveling the underlying

processes of deformation. This is because geometric approximation of final or intermediate structures, stipulation of generally ad hoc types of motion within a body, and a lack of explicit dependence upon causal elements such as applied loads, stress equilibrium, and constitutive relations, sensu stricto, are theoretically at odds with a complete mechanics.

We propose, as a goal for the 21st century, a significant revision of the educational objectives for courses in structural geology and tectonics, so that students are prepared to use the full complement of mechanical tools necessary to design a plan for field data collection, set up and solve relevant boundary-value problems, and evaluate the correspondence between models and data.

Acknowledgements

The incremental steps of normal science require a basis and a context—our basis is that established by the great mechanicians of the past two centuries; our context for the study of chevron folds and échelon veins is that largely established through the creative research, transparent writing, and indomitable spirit of John G. Ramsay, all of which are gratefully acknowledged here. Also, we take this opportunity to acknowledge the care and tenacity with which the former Editor of the *Journal of Structural Geology*, Sue Treagus, has so ably monitored and promoted this journal and the discipline of structural geology for the past decade. RCF was supported by NSF Grant EAR 9526983.

References

Atkinson, B.K., Meredith, P.G., 1987. Experimental fracture mechanics data for rocks and minerals. In: Atkinson, B.K. (Ed.), Fracture Mechanics of Rock. Academic Press, London, pp. 477–525.

Barenblatt, G.I., Joseph, D.D., 1996. In: Collected Papers of R.S. Rivlin. Springer, New York, p. 2827.

Bayly, M.B., 1964. A theory of similar folding in viscous materials. American Journal of Science 262, 753–766.

Bayly, M.B., 1970. Viscosity and anisotropy estimates from measurements on chevron folds. Tectonophysics 9, 459–474.

Bayly, M.B., 1976. Development of chevron folds: discussion. Geological Society of America Bulletin 87, 1664.

Bayly, M.B., Cobbold, P.R., 1979. Simple deviation of shortening/rotation relation for straight limbs on symmetrical folds. Tectonophysics 53, T1–T5.

Beach, A., 1975. The geometry of en échelon vein arrays. Tectonophysics 28, 245–263.

Biot, M.A., 1965a. Theory of similar folding of the first and second kind. Geological Society of America Bulletin 76, 251–258.

Biot, M.A., 1965b. Further development of the theory of internal buckling of multilayers. Geological Society of America Bulletin 76, 833–840.

Casey, M., 1980. Mechanics of shear zones in isotropic dilatant materials. Journal of Structural Geology 2, 143–147.

Casey, M., Huggenberger, P., 1985. Numerical modeling of finite-amplitude similar folds developing under general deformation histories. Journal of Structural Geology 7, 103–114.

Chapple, W.M., Spang, J.H., 1974. Significance of layer-parallel slip during folding of layered sedimentary rocks. Geological Society of America Bulletin 85, 1523–1534.

Chester, J., Fletcher, R.C., 1997. Stress distribution and failure in anisotropic rock near a bend in a weak fault. Journal of Geophysical Research 102, 693–708.

Clark, P. Jr., 1966. Handbook of physical constants. Geological Society of America Memoirs.

Cloos, E., 1955. Experimental analysis of fracture patterns. Geological Society of America Bulletin 66, 241–258.

Cobbold, P.R., 1976. Mechanical effects of anisotropy during large finite deformations. Bulletin of the Society of Geologists, France 18, 1497–1510.

Collins, D.A., De Paor, D.G., 1986. A determination of the bulk rotational deformation resulting from displacements in discrete shear zones in the Hercyniam Fold Belt of South Ireland. Journal of Structural Geology 8, 101–109.

Craddock, J.P., van der Pluijm, B.A., 1988. Kinematic analysis of an en échelon-continuous vein complex. Journal of Structural Geology 10, 445–452.

Crider, J.G., Pollard, D.D., 1998. Fault linkage: three-dimensional mechanical interaction between échelon normal faults. Journal of Geophysical Research 103, 24,373–24,391.

Crouch, S.L., Starfield, A.M., 1983. Boundary element methods in solid mechanics. George Allen and Unwin, London.

Dahlstrom, C.D.A., 1969. Balanced cross sections. Canadian Journal of Earth Science 6, 743–757.

de Sitter, L.U., 1956. Structural Geology. McGraw-Hill, London.

Engelder, T., 1987. Joints and shear fractures in rock. In: Atkinson, B.K. (Ed.), Fracture Mechanics of Rock. Academic Press, London, pp. 27–69.

Erdogan, F., Sih, G.C., 1963. On the crack extension in plates under plane loading and transverse shear. Journal of Basic Engineering—Transactions of American Society of Mechanical Engineers 85, 519–527.

Fletcher, R.C., Pollard, D.D., 1981. Anticrack model for pressure solution surfaces. Geology 9, 419–424.

Granier, T., 1985. Origin, damping, and pattern development of faults in granite. Tectonics 4, 721–737.

Gray, D.R., Durney, D.W., 1979. Crenulation cleavage differentiation: implications of solution-deposition processes. Journal of Structural Geology 1, 73–80.

Hancock, P.L., 1972. The analysis of en échelon veins. Geological Magazine 109, 269–276.

Hudleston, P.J., 1973. Fold morphology and some geometric implications of theories of fold development. Tectonophysics 16, 1–46.

Ingraffea, A.R., 1981. Mixed-mode fracture initiation in Indiana limestone and Westerly granite. Proceedings of the 22nd U.S. Symposium on Rock Mechanics, MIT, Boston MA, Einstein, H.H., (Ed.). MIT, Cambridge, MA, pp. 186–191.

Jaeger, J.C., Cook, N.G.W., 1969. Fundamentals of Rock Mechanics. Methuen.

Johnson, A.M., Fletcher, R.C., 1994. Folding of viscous layers: mechanical analysis and interpretation of structures in deformed rock. Columbia University Press, New York.

Johnson, A.M., Pfaff, V.J., 1989. Parallel, similar and constrained folds. Engineering Geology 27, 115–180.

Kanninen, M.F., Popelar, C.H., 1985. Advanced fracture mechanics. Oxford University Press, New York.

Knipe, R.J., White, S.H., 1979. Deformation in low grade shear zones in the Old Red Sandstone, S.W. Wales. Journal of Structural Geology 12, 53–66.

Lajtai, E.Z., 1969. Mechanics of second order faults and tension gashes. Geological Society of America Bulletin 80, 2253–2272.

Lawn, B.R., Wilshaw, T.R., 1975. Fracture of brittle solids. Cambridge University Press, Cambridge.

Nicholson, R., Ejiofor, I.B., 1987. The three-dimensional morphology of arrays of échelon and sigmoidal, mineral-filled fractures: data from North Cornwall. Geologic Sociey of London Journal 144, 79–83.

Nicholson, R., Pollard, D.D., 1985. Dilation and linkage of échelon cracks. Journal of Structural Geology 7, 583–590.

Olson, J., Pollard, D.D., 1989. Inferring paleostresses from natural fracture patterns: a new method. Geology 17, 345–348.

Olson, J.E., Pollard, D.D., 1991. The initiation and growth of en échelon veins. Journal of Structural Geology 13, 595–608.

Pfaff, V.J., Johnson, A.M., 1989. Opposite senses of fold asymmetry. Engineering Geology 27, 3–38.

Pollard, D.D., Segall, P., Delaney, P.T., 1982. Formation and interpretation of dilatant échelon cracks. Geological Society of America Bulletin 93, 1291–1303.

Ramsay, J.G., 1967. Folding and fracturing of rocks. McGraw-Hill, New York.

Ramsay, J.G., 1974. Development of chevron folds. Geological Society of America Bulletin 85, 1741–1754.

Ramsay, J.G., 1980. The crack–seal mechanism of rock deformation. Nature 284, 135–139.

Ramsay, J.G., Huber, M.I., 1983. The techniques of modern structural geology, Volume I: Strain Analysis. Academic Press, London.

Ramsay, J.G., Huber, M.I., 1987. Folds and fractures. In: The Techniques of Modern Structural Geology, 2. Academic Press, London.

Rickard, M.J., Rixon, L.K., 1983. Stress configurations in conjugate quartz-vein arrays. Journal of Structural Geology 5, 573–578.

Riedel, W., 1929. Zur mechanik geologischer Brucherscheinungen (Ein Beitrag zum Problem der Fiederspatten). Centralblatt für Mineralogie, Geologie und Paläontologie B, 354–368.

Roering, C., 1968. The geometrical significance of natural en échelon crack arrays. Tectonophysics 5, 107–123.

Rothery, E., 1988. En échelon vein array development in extension and shear. Journal of Structural Geology 10, 63–71.

Shainin, V.E., 1950. Conjugate sets of en échelon tension fractures in the Athens limestone at Riverton, Virginia. Geological Society of America Bulletin 61, 509–517.

Shaoxun, H., Xiaoshuang, X., 1988. The origin of échelon structures of Tungsten veins in Xishuashan, Jiangxi. Acta Geologica Sinica 1, 267–280.

Smith, J.V., 1995. True and apparent geometric variability in en-échelon vein arrays. Journal of Structural Geology 17, 1621–1626.

Smith, J.V., 1996. En échelon sigmoidal vein arrays hosted by faults. Journal of Structural Geology 18, 1173–1179.

Smith, J.V., 1997. Initiation of convergent extension fracture vein arrays by displacement of discontinuous fault segments. Journal of Structural Geology 19, 1369–1373.

Sommer, E., 1969. Formation of fracture 'lances' in glass. Engineering Fracture Mechanics 1, 539–546.

Thomas, A.L., Pollard, D.D., 1993. The geometry of échelon fractures in rock: implications from laboratory and numerical experiments. Journal of Structural Geology 15, 323–334.

Timoshenko, S.P., Goddier, J.N., 1970. Theory of Elasticity. McGraw-Hill Book Company, New York.

White, F.M., 1974. Viscous fluid flow. McGraw-Hill Book Company, New York.

Williams, J.R., 1980. Similar and chevron folds in multilayers using finite-element and geometric models. Tectonophysics 65, 323–338.

Wilson, G., 1952. A quartz vein system in the Moine Series near Melness, A'Mhoine, North Sutherland, and its tectonic significance. Geological Magazine 89, 141–144.